Toxicological assessment of commercial monolayer tungsten disulfide nanomaterials aqueous suspensions using human A549 cells and the model fungus *Saccharomyces cerevisiae*

Brixhilda Domi [a], Kapil Bhorkar [b, c], Carlos Rumbo [a], Labrini Sygellou [b], Sonia Martel Martin [a], Roberto Quesada [d], Spyros N. Yannopoulos [b], Juan Antonio Tamayo-Ramos [a, *]

[a] International Research Centre in Critical Raw Materials-ICCRAM, Universidad de Burgos, Plaza Misael Banuelos S/n, 09001, Burgos, Spain
[b] Foundation for Research and Technology Hellas, Institute of Chemical Engineering Sciences (FORTH/ICE-HT), P.O. Box 1414, GR-26504, Rio-Patras, Greece
[c] Univ Rennes, CNRS, ISCR, UMR 6226, F-35000, Rennes, France
[d] Departamento de Química, Facultad de Ciencias, Universidad de Burgos, 09001, Burgos, Spain

HIGHLIGHTS

- Commercial 2D WS_2 aqueous suspensions with different lateral size where characterized.
- The suspensions were composed by a combination of 1T′-WS_2, 2H-WS_2, WO_3 and SO_2.
- Both commercial samples showed no reduction on cellular vitality in A549 cells.
- Both commercial samples reduced the cellular vitality of *Saccharomyces cerevisiae*.

GRAPHICAL ABSTRACT
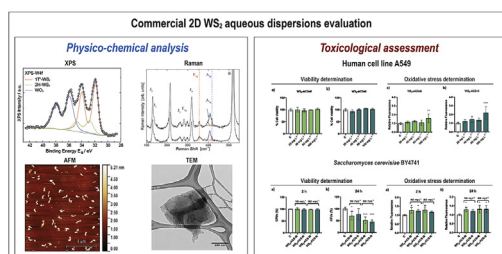
ARTICLE INFO

ABSTRACT

The utilization of tungsten disulfide (WS_2) nanomaterials in distinct applications is raising due to their unique physico-chemical properties, such as low friction coefficient and high strength, which highlights the necessity to study their potential toxicological effects, due to the potential increase of environmental and human exposure. The aim of this work was to analyze commercially available aqueous dispersions of monolayer tungsten disulfide (2D WS_2) nanomaterials with distinct lateral size employing a portfolio of physico-chemical and toxicological evaluations. The structure and stoichiometry of monolayer tungsten disulfide (WS_2-ACS-M) and nano size monolayer tungsten disulfide (WS_2-ACS-N) was analyzed by Raman spectroscopy, whereas a more quantitative approach to study the nature of formed oxidized species was undertaken employing X-ray photoelectron spectroscopy. Adenocarcinomic human alveolar basal epithelial cells (A549 cells) and the ecotoxicology model *Saccharomyces cerevisiae* were selected as unicellular eukaryotic systems to assess the cytotoxicity of the nanomaterials. Cell viability and reactive oxygen species (ROS) determinations demonstrated different toxicity levels depending on the cellular model used. While both 2D WS_2 suspensions showed very low toxicity towards the A549 cells, a comparable concentration (160 mg L^{-1}) reduced the viability of yeast cells. The toxicity of a nano size 2D WS_2 commercialized in dry form from the same provider was also assessed, showing ability to reduce yeast cells viability as well. Overall, the presented data reveal the physico-chemical properties and the

---

* Corresponding author.
   E-mail addresses: jatramos@ubu.es, ja.tamayoramos@gmail.com (J.A. Tamayo-Ramos).

potential toxicity of commercial 2D WS2 aqueous suspensions when interacting with distinct eukaryotic organisms, showing differences in function of the biological system exposed.

1. Introduction

Monolayer tungsten disulfide (2D WS$_2$) nanomaterials are standing out within the transition metal dichalcogenides (TMDs) family due to their unique physico-chemical properties and to the more favorable commercial availability of W, when compared to other transition metals with similar properties (Eftekhari, 2017). WS$_2$ has shown potential for applications in different industrial settings for the production of transistors, sensors or photocatalytic and electronic devices (Choi et al., 2017). Since WS$_2$ exhibits both low friction coefficient and high strength, it also represents an excellent dry lubricant (Ratoi et al., 2013). Furthermore, as a result of the low friction coefficient, tungsten disulfide is used in clinical dentistry for orthodontic implants (Katz et al., 2006). In addition, WS$_2$ is currently being used in manufacturing, marine, agriculture, and automotive applications (Eftekhari, 2017). As a consequence of the increased use of WS$_2$, there is also the necessity to study the potential toxicological effects of this material, due to the potential increase of environmental and human exposure. Given the rapid increases in the production volumes of these nanomaterials, with novel technologies for large-scale synthesis being developed (Sharma et al., 2020), and their incorporation into multiple and new applications, it can be reasonably assumed that releases of 2D WS$_2$ into the environment will be increasing accordingly from multiple pathways. These include point source emissions, such as those from industrial installations or from urban waste-water treatment plants, and diffuse source emissions, i.e. emissions from products along their life cycle, which may provoke human and ecosystems exposures to a large range of potential nanomaterial concentrations.

The structures of exfoliated TMD materials are very different to those exhibited by conventional bulk structures (Jeevanandam et al., 2018), and even though all TMDs exhibit similar layered 2D morphology, their biocompatibility can be significantly altered depending on several parameters such size, shape or the method used to prepare the 2D TMD nanosheets (Lv et al., 2015). The toxicity of WS$_2$ nanomaterials is yet understudied, only a limited number of toxicological studies are available using distinct eukaryotic and prokaryotic models (Appel et al., 2016; Liu et al., 2017; Yuan et al, 2018, 2020). For instance, Appel et al. studied the potential toxicological effects of WS$_2$ nanoparticles prepared by several methods such as mechanical exfoliation and chemical vapor deposition (CVD) toward human epithelial kidney cells (HEK293f) (Appel et al., 2016), while other authors focused on the evaluation of the impact of commercial 2D WS$_2$ powders on the viability of other human cell lines, such as NL-20, HEPG2 and macrophages (Corazzari et al., 2014; Pardo et al., 2014). The potential synergistic toxic effects on different human cell lines (RAW264.7 and A549) of WS$_2$ nanosheets and organic pollutants have been reported recently as well, showing their capability to damage the plasma membrane and cytoskeleton, resulting in increased membrane permeability and enhanced organic pollutant uptake (Yuan et al., 2020). Moreover, molecular dynamics simulations suggest the ability of WS$_2$ nanosheets to disturb the secondary structure of efflux pumps, hampering xenobiotics elimination (Yuan et al., 2020). The biological responses of Gram-negative *Escherichia coli* and Gram-positive *Staphylococcus aureus* to WS$_2$ nanosheets have

been reported as well, indicating a time and concentration dependent antibacterial activity for both bacterial strains (Liu et al., 2017). The potential toxic effects of chemically exfoliated WS$_2$ nanosheets (Ce-WS$_2$) and annealed exfoliated WS$_2$ nanosheets (Ae-WS$_2$, 2H phase) were investigated toward the single-celled green algae *Chlorella vulgaris*, where differences in the toxicity of both nanomaterials towards the microorganism were observed, possibly due to differences in the physico-chemical parameters of the two materials (Yuan et al., 2018). Notably, while recently we have observed that molybdenum disulfide (MoS$_2$) nanomaterials exert a negative impact on the viability of the yeast *Saccharomyces cerevisiae* (Domi et al., 2020a), no reports are available yet about the effect of WS$_2$ nanomaterials on yeast or other fungal species. Thus, in the present work, we explored the *in vitro* cytotoxicity of commercial 2D WS$_2$ materials in two different eukaryotic models: human alveolar carcinoma epithelial cells A549 to mimic the potential hazard *via* inhalation exposure (Lanone et al., 2009; Visalli et al., 2015) and the yeast *S. cerevisiae*, as a well-established model in ecotoxicology, to investigate their potential impact in fungi (Braconi et al., 2016; Mell and Burgess, 2002; Michels, 2003).

2. Materials and methods

2.1. Materials and reagents

Chemicals employed were purchased from Sigma-Aldrich (Merck KGaA, Darmstadt, Germany) and Acros Organics (Thermo Fisher Scientific Inc., Madrid, Spain). Monolayer tungsten disulfide water dispersion (WS$_2$-ACS-M, ref: GLWSW0A2), and nano size monolayer tungsten disulfide water dispersion (WS$_2$-ACS-N, ref: GLMSWNA2) and dry powder (WS$_2$-ACS-N-PW, ref: MOS2PN002) forms were purchased at ACS material®.

2.2. Physico-chemical characterization of 2D WS$_2$ aqueous suspensions

2.2.1. Atomic force microscopy (AFM) and transmission electron microscopy (TEM) analysis

AFM images were recorded in tapping mode with an Alpha300R-Alpha300A AFM Witec instrument, using Arrow NC cantilevers with a tip radius <10 nm and a force constant of 42 N/m. All the WS$_2$ samples were placed on a mica surface from aqueous solutions by drop casting. TEM analysis was performed at the microscopy unit from the University of Valladolid, using a JEOL JEM-1011 high-resolution (HR) TEM coupled with a Gatan Erlangshen ES1000W camera. Samples were deposited on Lacey Carbon Type-A, 300 mesh, copper grids.

2.2.2. Raman spectroscopy

Raman spectra were excited by the 441.6 nm radiation emerging from a He−Cd laser (Kimon). The laser light was focused by a 50 × objective creating a focusing area of 2−3 μm. The scattered light was collected by the same objective and analyzed using by the LabRam HR800 (Jobin-Yvon) spectrometer operating at a spectral resolution of ~2.0 cm. A very low light fluence (275 μW) on the sample was used to avoid heat induced effects (oxidation and decomposition). The Raman mode of Si single crystal at 520 cm-1

was used to calibrate the wavenumber scale of the spectra.

2.2.3. X-ray photoelectron spectroscopy

The surface analysis measurements were performed in a UHV chamber (P~5 $\times$ 10^{-10} mbar) equipped with a SPECS Phoibos 100-1D-DLD hemispherical electron analyzer and a non-monochromatized dual-anode Mg/Al x-ray source for XPS. The spectra were recorded with AlKα at 1486.6 eV photon energy using analyzer pass energy of 10 eV which results to full width at half maximum (FWHM) of 0.85 eV for Ag3d5/2 line. The analyzed area was a rectangle with dimensions 7x15 mm^2. Spectra were accumulated and processed using SpecsLab Prodigy (Specs GmbH, Berlin) software. The XPS peaks were deconvoluted with mixed Gaussian $-$ Lorentzian functions after a Shirley background subtraction. The WS$_2$-ACS-M and WS$_2$-ACS-N samples were prepared by drop casting the dispersion on Si wafers, whereas powder of the WS$_2$-ALK-N was pressed on Indium foil.

2.3. A549 cell culture

The human alveolar carcinoma epithelial cell line A549 (ATCC, CCL-185) were grown in DMEM medium (Dulbecco's Modified Eagle Medium) supplemented with 10% foetal calf serum (FCS) and 1% penicillin/streptomycin (Sigma-Aldrich). Cells were grown in a humidified incubator at 37 °C and 5% CO$_2$.

2.4. A549 cells neutral red assay

To assess the potential toxicity of the selected commercial 2D WS$_2$ products, human lung carcinoma A549 cells were exposed to 20, 40, 80 and 160 mg L^{-1} of WS$_2$-ACS-M and WS$_2$-ACS-N, for a period of 24 h. Around 3 $\times$ 10^4 cells were incubated in culture media with 5% CO$_2$ for 24 h at 37 °C. Then, A549 cells were seeded in 96 well plates and exposed to the mentioned nanomaterials concentrations, diluted in DMEM 1% FCS. Cells were incubated as well with medium having the same composition in the absence of nanomaterials (control cells). After 24 h of exposure, cells were washed and incubated with 100 μL of the Neutral Red solution which was prepared as follows: neutral red stock (4 mg L^{-1}) was diluted 1:100 in treatment media then incubated for 24 h at 37 °C protected from light. After 2.5 h incubation, cells were washed once with DPBS and fixed with formaldehyde 4%. Then, cells were washed again with DPBS and a solution of extraction (50% ethanol 96°, 49% distilled H$_2$O and 1% acetic acid) was added to all wells. After 10 min of moderate shaking, this solution was transferred to a new opaque 96-well plate, and fluorescence was measured with a microplate reader (BioTek Synergy HT, excitation wavelength, 530/25; emission wavelength 645/40). Results were expressed as percentage of control (absorbance of cells in absence of materials). Two independent experiments were done, employing 3 replicates per exposure condition tested in each case.

2.5. A549 cells ROS determination

2,7-dichlorofluorescin diacetate (DCFH-DA) was used to perform quantitative measurements of oxidative stress production via intracellular reactive oxygen species (ROS). Around 3 $\times$ 10^4 cells per well were seeded in a 96 micro-well plate and labeled for 30 min with 50 μM DCFH-DA in Hanks' Balanced Salt Solution (HBSS). After the incubation, cells were washed once with HBSS and several (20, 40, 80 and 160 mg L^{-1}) concentrations of the nanomaterials (diluted in HBSS) were added to each well. Fluorescence was measured with a microplate reader (BioTek Synergy HT, excitation wavelength, 530/25; emission wavelength 645/40) after 1 h of incubation. Two independent experiments were done,

employing 3 replicates per exposure condition tested in each case.

2.6. Yeast culture

The yeast *S. cerevisiae* BY4741 strain was utilized to perform toxicological assays and was grown in standard liquid YPD medium (1% yeast extract, 1% yeast bacto-peptone, 2% glucose). Cells were cultured in liquid media on a rotary shaker at 185 rpm at 30 °C.

2.7. Yeast colony forming units (CFUs) determination

Yeast cells in exponential growth phase (OD$_{600}$ = 1) were incubated with different 2D WS$_2$ samples at 160 and 800 mg L^{-1} in 1 mL cultures in 24 well plates. The cultures were sampled at two different exposure times (2 and 24 h), and colony forming units determination was done by inoculating adequate dilutions in solid YPD medium plates, which were incubated at 30 °C for 48 h. Two independent experiments were done, employing 3 replicates per exposure condition tested in each case.

2.8. Yeast ROS assay

The reagent CM-H2DCFDA (Invitrogen, General Oxidative Stress Indicator) was utilized to determine ROS in yeast following a protocol similar to that reported by James et al.[24] *S. cerevisiae* cells growing in exponential phase were pelleted, washed and incubated with CM-H2DCFDA (7 μM) in DPBS for 60 min at 30 °C and 185 rpm. Consequently, yeast cells were washed, suspended in YPD medium and thus exposed to the three WS$_2$ samples (160 and 800 mg L^{-1}) for 2 and 24 h. Next, cells were washed two times with DPBS, incubated 2 min in a solution containing lithium acetate 2 M, washed again and incubated for 2 min in a solution containing SDS (sodium dodecyl sulfate) (0.01%) and chloroform (0.4%). Finally, cells were pelleted and the supernatant was transferred to a black opaque 96 micro-well plate, where the fluorescence was measured (excitation = 485; emission = 528) using a microplate reader (Synergy-HT, BioTek). Two independent experiments were done, employing 3 replicates per exposure condition tested in each case.

2.9. Statistical analysis

Statistical analysis data are shown as means ± SD. Differences between the negative control and exposure conditions were established using one-way analysis of variance (ANOVA) for multiple comparisons, followed by Dunnet *post hoc* test. Statistical tests were carried out using Prism 6.0 (GraphPad Prism, GraphPad Software, Inc.). *P* values of less than 0.05 were considered to indicate statistical significance.

3. Results and discussion

3.1. Selection and characterization of commercial 2D tungsten disulfide

Initially, we selected two commercial 2D WS$_2$ aqueous suspensions from ACS material®, namely monolayer tungsten disulfide (WS$_2$-ACS-M) ("M" standing for "micro"), with a lateral size ranging from 100 nm to 4 μm, and nano size monolayer tungsten disulfide (WS$_2$-ACS-N) ("N" standing for "nano"), with a narrower and smaller lateral size distribution (20−500 nm). To confirm their morphologic characteristics AFM and TEM analyses were performed by drop casting the samples on mica surfaces and carbon-coated copper grids respectively (Fig. 1). The AFM images gave insights into the particle size distribution and shape of both nanomaterial types, showing similarities to previously reported AFM
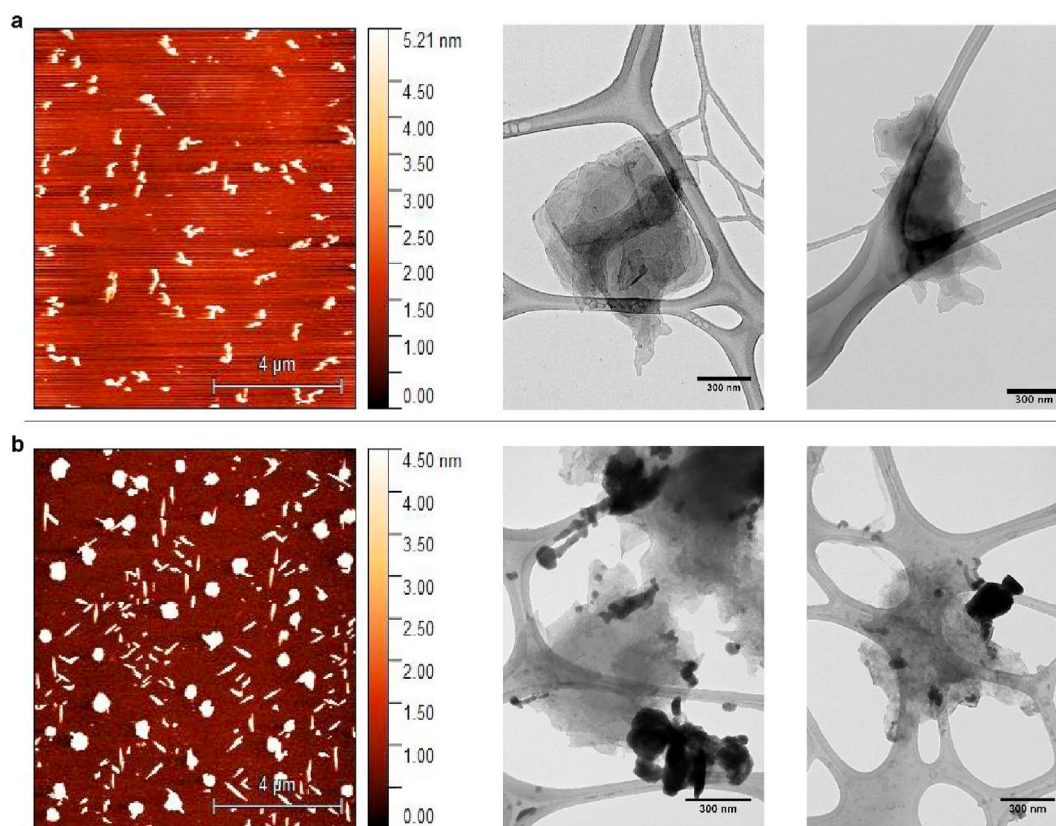
Fig. 1. AFM and TEM images of WS$_2$-ACS-M (a) and WS$_2$-ACS-N (b). Tungsten disulfide dispersions with a concentration of 20 mg L^{-1} were deposited by drop casting on mica surfaces and carbon-coated copper grids respectively.

images of WS$_2$ nanomaterials (Štengl et al., 2014; Zirak et al., 2015). The TEM analysis images indicated that both nanomaterials have a platelet-like morphology, as expected considering the supplier information. However, considering both AFM and TEM images, no clear differences between the two products could be observed in terms of size, aggregation state or morphological characteristics.

To analyze the structure and stoichiometry of the materials, X-ray photoelectron spectra (XPS) and Raman spectra of the samples were collected and analyzed. In relation to the XPS analysis, Fig. 2a—b shows the W4f spectra of WS$_2$-ACS-M and WS$_2$-ACS-N, respectively. The spectra consist of three doublets with a spin orbit splitting W4f$_{7/2}$-W4f$_{5/2}$ of ~2.0 eV. The binding energies (BE) of the W4f$_{7/2}$ components obtained by the fitting analysis are located at 31.9, 32.8 and 35.9 eV, which are assigned to the phases 1T'-WS$_2$, 2H-WS$_2$, and the WO$_3$ oxide, respectively (Liu et al., 2018). Deconvoluted XP spectra of the S2p peak are shown in Fig. 2c—d. The XP spectra of both materials are analyzed into three doublets with a spin orbit splitting S2p$_{3/2}$-S2p$_{1/2}$ of ~1.2 eV. The binding energies of S2p$_{3/2}$ components located at ~161.6, ~162.5 and ~168.0 eV, are assigned to 1T'-WS$_2$, 2H-WS$_2$ (Liu et al., 2018), and to sulphonyl groups (—SO$_2$— groups) (Marletta and Iacona, 1996), respectively. The relative fraction of the various components, corresponding to the W and S species identified by the fitting analysis are shown in Table 1.

Raman spectra for the 2D WS$_2$ samples are shown in Fig. 3. The vertical dashed lines represent the energies of the in-plane E_{2g}^1 and out-of-plane A_{1g} symmetries of the 2H-WS$_2$ phase located at 356 and 417.5 cm^{-1}, respectively (Berkdemir et al., 2013). The spectrum of WS$_2$-ACS-M and WS$_2$-ACS-N exhibit the mentioned bands, albeit as weak features. A strong band near 408 cm^{-1} overwhelms the

intensity of the A_{1g} mode; hence, a fitting analysis was performed to identify the correct energy of the A_{1g} band. Typical examples of the fitting for the spectra of both the WS$_2$-ACS-M and WS$_2$-ACS-N samples are shown in Fig. 3. The peak energies and their differences of the E_{2g}^1 and A_{1g} bands suggest the existence of monolayer WS$_2$ for both samples. In line with XPS analysis, the weak intensity of the 2H-WS$_2$, indicates a rather small relative fraction of this phase, in comparison to other phases present in WS$_2$-ACS-M and WS$_2$-ACS-N. Indeed, a number of additional strong bands emerge in the Raman spectra of the selected 2D WS$_2$ samples. As the current excitation (441.6 nm) is far from resonance conditions (514.5 nm), the additional Raman bands cannot be assigned to resonance bands. Based on the XPS analysis, which revealed the presence of the 1T'-WS$_2$ phase and WO$_3$ oxide, we attempt a Raman band assignment based on these two phases. A number of vibrational bands have been observed in the Raman spectrum of the 1T'-WS$_2$ phase (Tan et al., 2017). These bands are labeled as J$_1$ (139 cm^{-1}) J$_2$ (133 cm^{-1}) J$_3$ (265 cm^{-1}) and J$_4$ (321 cm^{-1}). All these bands are observed also in the current spectra, albeit with a red-shift of 2—3 cm^{-1}. For both WS2-ACS-M and WS2-ACS-N samples, the metallic phase (1T') was found to be the dominant one in relation to the semiconducting phase (2H).

3.2. Toxicology assessment using adenocarcinoma A549 human cells

To study the percentage of the surviving cells after the incubation with the nanomaterials, the Neutral Red assay was chosen as a very common cytotoxicity test for the evaluation of the potential toxicity of nanoparticles (Repetto et al., 2008). The assay allows the
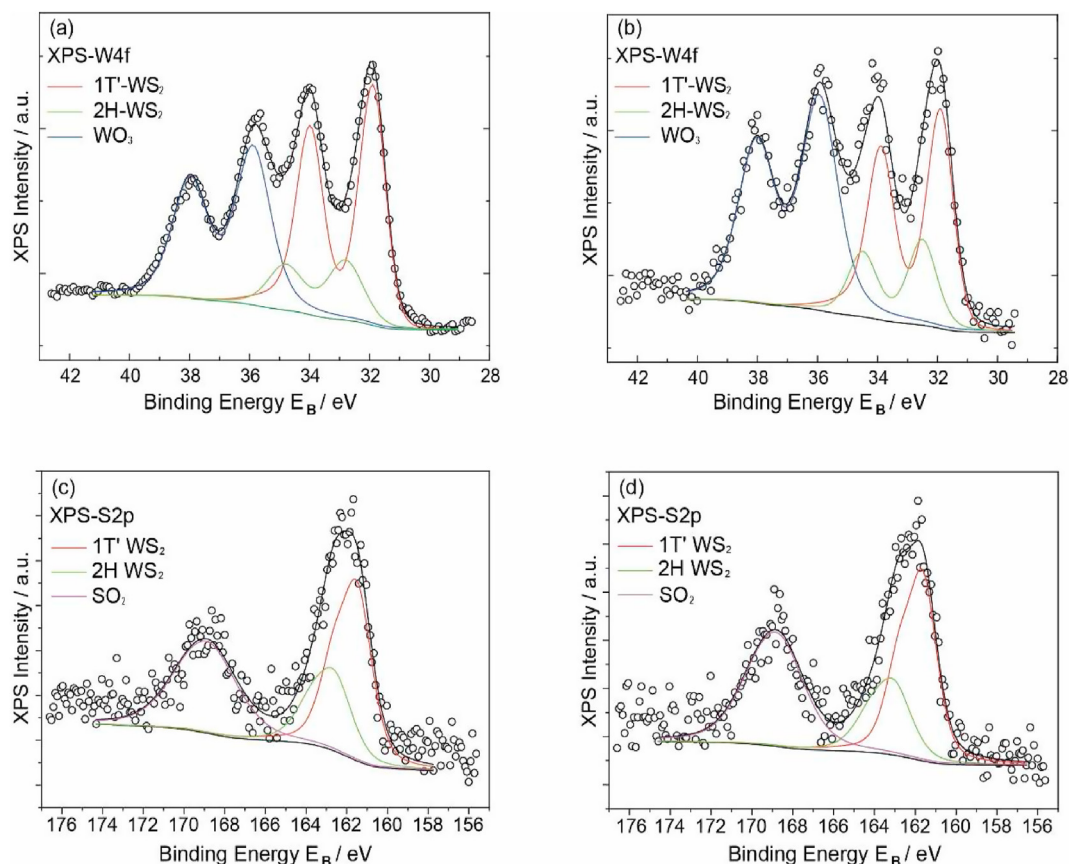
Fig. 2. De-convoluted W4f spectra of (a) WS$_2$-ACS-M, and (b) WS$_2$-ACS-N, and deconvoluted S2p XPS spectra of (c) WS$_2$-ACS-M, and (d) WS$_2$-ACS-N samples.

Table 1
Relative fraction of the 2D WS$_2$ aqueous dispersions components, corresponding to the W and S species identified.

% concentration of WS$_2$ phases and WO$_3$			
	1T′-WS$_2$	2H-WS$_2$	WO$_3$
WS$_2$-ACS-M	47.7 ± 0.7	13.9 ± 0.7	38.3 ± 0.7
WS$_2$-ACS-N	38.7 ± 0.8	14.5 ± 0.8	46.8 ± 0.8
% concentration of WS$_2$ phases and SO$_2$			
	1T′-WS$_2$	2H-WS$_2$	SO$_2$
WS$_2$-ACS-M	42.8 ± 0.7	21.8 ± 0.7	35.5 ± 0.7
WS$_2$-ACS-N	41.8 ± 0.8	19.6 ± 0.8	38.6 ± 0.8

relative quantification of living cells in a culture, due to the capability of vital cells to absorb the Neutral Red dye, following the accumulation into the cellular lysosomes. The results obtained after a 24 h exposure to both 2D WS$_2$ nanomaterial types are displayed in Fig. 4.

As it can be observed, the viability of the A549 cells was not reduced in the presence of the different concentrations tested. Few studies have assessed the toxicological effects of different WS$_2$ nanomaterials toward lung epithelial cells, reporting in some cases opposite results. While the work of Teo et al. indicated low cytotoxicity of exfoliated WS$_2$ nanosheets using thiazolyl blue tetrazolium bromide (MTT) and water-soluble tetrazolium salt (WST-8) assays in concentrations up to 400 mg L^{-1}, Liu et al. observed an evident negative impact of WS$_2$ nanoparticles on A549 cells with concentrations of 50 mg L^{-1} or higher, employing the CCK-8 assay. However, in concordance with the results obtained in the present work, most of the studies testing the toxicity of different TMD nanoforms, including WS$_2$, indicate a low degree of cytotoxicity towards respiratory models and other human cell lines (Appel et al.,

2016; Corazzari et al., 2014; Pardo et al., 2014; Teo et al., 2014).

Although the WS$_2$ nanoparticles did not induce significant cell death, we aimed to study the possible generation of intracellular ROS triggered by these materials. ROS generation can result in cell damage, inflammation and several diseases and pathologies (Holmström and Finkel, 2014). Henceforth, as done previously in the Neutral Red viability assay, we determined the ROS generation after the cell's exposure during 1 h to different concentrations from 20 to 160 mg L^{-1} of the 2D WS$_2$ samples (Fig. 5).

The ROS levels observed in the different conditions tested remained at relatively low level in comparison with the non-treated cells condition. This result is similar to that observed as well in exposed A549 cells by Corazzari et al., where the presence of WS$_2$ fullerene-like spherical engineered nanomaterials did not induce oxidative stress at different concentrations (Corazzari et al., 2014). The exposure of other human unicellular models, such as human kidney cells (HEK293f), nontumorigenic human bronchial epithelial cells (NL-20) and human liver carcinoma cells (HepG2) to different WS$_2$ nanoforms has produced similar results to those
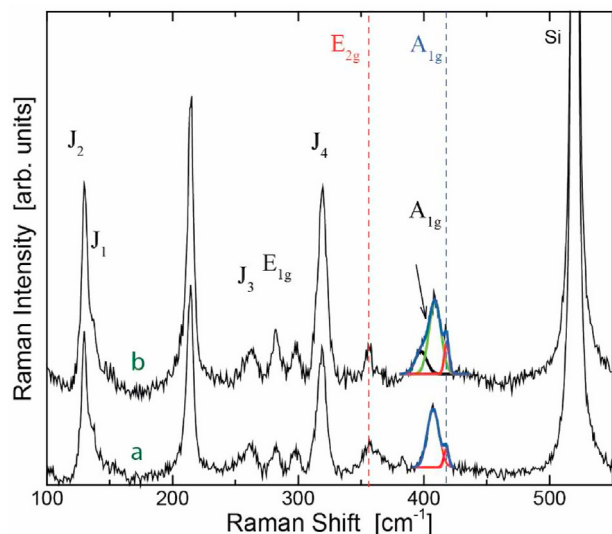
Fig. 3. Raman spectra of WS$_2$-ACS-M (a) and WS$_2$-ACS-N (b) samples.

observed in the present work, where low cytotoxicity levels were observed (Appel et al., 2016; Pardo et al., 2014). Also, by comparing the obtained results with those from previous studies where we have assessed the potential toxicity of distinct commercial bidimensional nanomaterials, such as graphene oxide or molybdenum disulfide, employing the same exposure conditions as those described here, it can be observed that the low toxicity displayed by the selected 2D WS$_2$ nanomaterials is comparable to that observed for 2D MoS$_2$ (Domi et al., 2020b), while 2D graphene oxide showed to be less safe (Domi et al., 2019). These observations are in concordance with those made by other authors, that arrived to the same conclusion but employing materials from different sources and distinct toxicology assays (Chng and Pumera, 2015; Teo et al., 2014).

3.3. Toxicology assessment using S. cerevisiae

The yeast *S. cerevisiae* is a well-consolidated and widely used model organism utilized for the evaluation of cellular response to stress and ecotoxicology studies (Braconi et al., 2016; Ivask et al., 2014; Sousa et al., 2018). So far, no nanosafety studies are available on the cytotoxicity of WS$_2$ nanoforms on *S. cerevisiae*, while recently, 2D MoS$_2$ have been reported to exert a significant toxicological impact on yeast cells, at least when the nanoparticles concentration range is from 160 to 800 mg L^{-1} (Domi et al., 2020a). Thus, we decided to investigate the possible toxicological potential of commercial 2D WS$_2$ flakes toward yeast, using the same concentration range. One of the most used assays in toxicological analyses when using microorganisms as model organisms is the determination of the number of colony forming units (CFUs) (Kwolek-Mirek and Zadrag-Tecza, 2014). Normally, cell viability is defined as a percentage of living cells in a whole population after the exposure to a certain substance in a specific time of incubation. *S. cerevisiae* cells were exposed to WS$_2$-ACS-M and WS$_2$-ACS-N at the concentrations of 160 and 800 mg L^{-1} for 2 and 24 h. As displayed in Fig. 6, no significant differences in viability were observed in the selected exposure conditions after 2 h of exposure in the two concentrations tested for both samples, compared to the control of non-treated cells. However, after 24 h exposure, a significant decrease on the viability of yeast incubated with 2D WS$_2$ could be observed. Lower average CFUs were observed in the presence of both concentrations tested. In the presence of 160 mg L^{-1}, the statistical significance (P ≤ 0.05) of *S. cerevisiae* viability decrease was only evident for WS$_2$-ACS-M, probably due to the slightly lower average viability and smaller standard deviation observed when compared to the results obtained for WS$_2$-ACS-N in comparable conditions. However, the viability reduction and statistical significance (P ≤ 0.0001) of the nanomaterials cytotoxicity towards the model fungi were more evident in the presence of 800 mg L^{-1}, where the average percentage of surviving cells after the exposure to WS$_2$-ACS-M and WS$_2$-ACS-N was around 50%.

The molecular pathway of the programmed cell death is associated with the production of ROS in an extensive variety of organisms, including *S. cerevisiae* (Perrone et al., 2008). When the level of oxidative stress production overwhelms antioxidant defense systems, the cell redox homeostasis is altered, resulting in the oxidation of proteins, peroxidation of lipids, DNA alterations, leading to reduced cell viability (Perrone et al., 2008). It has been reported that a large variety of nanoparticles can induce ROS in
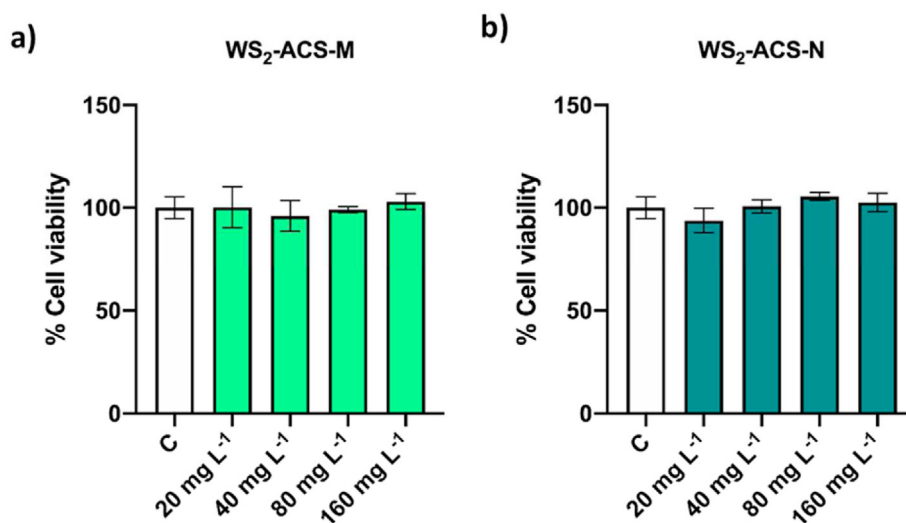

Fig. 4. Viability of A549 cells (Neutral Red assay) exposed to different concentrations of WS$_2$-ACS-M (a) and WS$_2$-ACS-N (b) for 24 h. Results are expressed as % of control (non-exposed cells). Data represent the mean (±standard deviation, SD) of two independent experiments. Differences were established using a One-way ANOVA followed by Dunnett *post hoc* test to compare every mean with the control. (For interpretation of the references to colour in this figure legend, the reader is referred to the Web version of this article.)
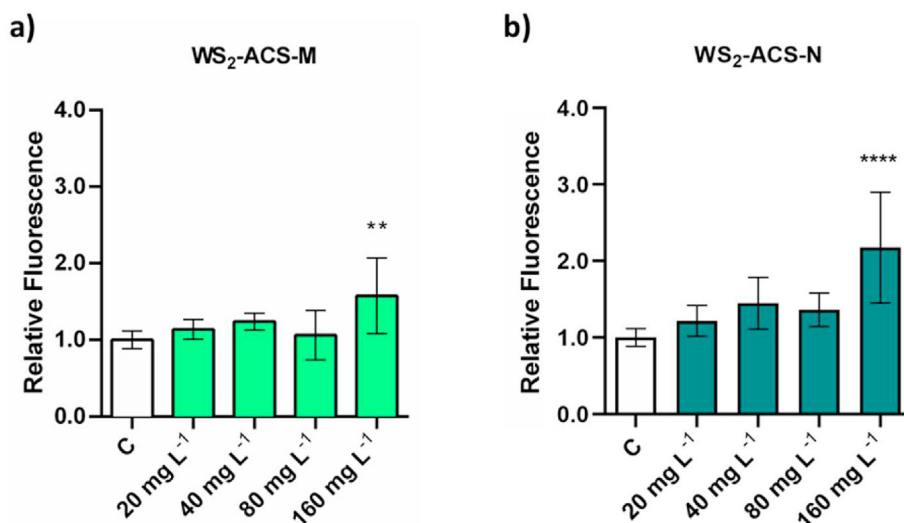
Fig. 5. ROS production of A549 cells treated with different concentrations of WS$_2$-ACS-M (a) and WS$_2$-ACS-N (b). The reported values are expressed as the relative fluorescence value to the control (untreated cells) which was assigned a value of 1. Data represent the mean of 2 independent experiments (±standard deviation, SD). Differences were established using a One-way ANOVA followed by Dunnett *post hoc* test to compare every mean with the control and considered significant at $P \leq 0.05$. ** $P \leq 0.01$, **** $P \leq 0.0001$.
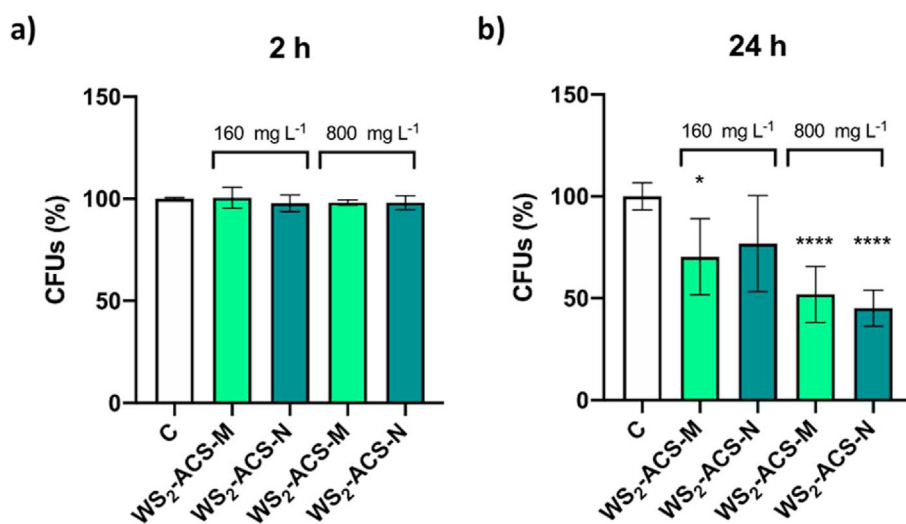

Fig. 6. CFUs determination of *S. cerevisiae* cells exposed to 160 and 800 mg L^{-1} of WS$_2$-ACS-M and WS$_2$-ACS-N during 2 (a) and 24 h (b). The reported values are the averages of two independent experiments. Differences were established using a One-way ANOVA followed by Dunnett *post hoc* test to compare every mean with the control, and considered significant at $P \leq 0.05$. * $P \leq 0.05$, **** $P \leq 0.0001$.

yeast, such as 2D MoS$_2$ (Domi et al., 2020a), graphene oxide (Domi et al., 2019), metalloid oxides (Sousa et al., 2019) and magnetic nanomaterials (Peng et al., 2018). Consequently, to understand whether the decrease of yeast viability could be associated to higher levels of oxidative stress, we analyzed ROS levels in cells exposed to WS$_2$. Hence, yeast cells were exposed to 160 and 800 mg L^{-1} of both commercial 2D WS$_2$ samples for 2 and 24 h. As shown in Fig. 7, oxidative stress levels in all exposure conditions were only slightly higher than those observed for the non-exposed cells, indicating a low capacity of the nanomaterials to induce the formation of intracellular ROS in yeast cells.

Interestingly, high concentrations (800 mg L^{-1}) of 2D nanomaterials, such as MoS$_2$ and graphene oxide, induced a clearer increase of ROS levels in yeast than those observed in the presence of 2D WS$_2$ (Domi et al, 2019, 2020a). This difference is particularly remarkable in case of graphene oxide, where commercial products from different suppliers induced 20 to 30 times higher ROS levels

compared to the non-treated cells condition.

In the present work, commercial aqueous suspensions of 2D WS$_2$ were selected due to their high nanoparticle dispersibility. Commercial 2D WS$_2$ dry powders, which are the most common commercialized form of the 2D nanomaterial, are obtained by drying 2D WS$_2$ aqueous suspensions that have been prepared through Li-intercalation and exfoliation in water. The copious gas evolution that occurs once water is added to Li$_x$WS$_2$ to induce 2D WS$_2$ exfoliation, enables the formation of highly dispersed, stable colloidal 2D WS$_2$ suspensions. However, when resuspending commercially available dry 2D WS$_2$ nanopowders in water to obtain aqueous suspensions, even when assisted by ultrasonication, the nanoparticle dispersion rate and the colloidal stability of the suspension obtained is lower (internal communication of the supplier). For this reason, we decided to test as well whether aqueous suspensions prepared in our laboratory, using the analogous version of nano size monolayer tungsten disulfide (WS2-ACS-N) in
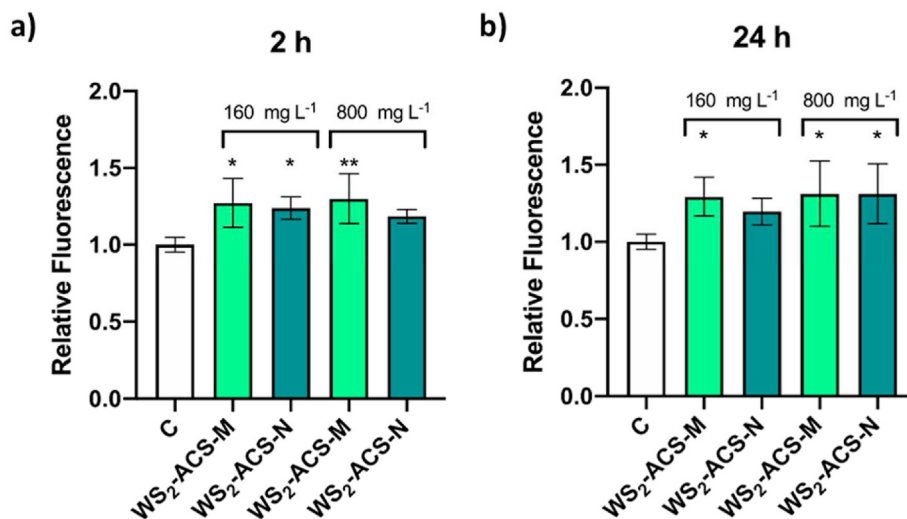
Fig. 7. Oxidative stress (ROS) determination of *S. cerevisiae* cells exposed to 160 and 800 mg L^{-1} of WS$_2$-ACS-M and WS$_2$-ACS-N during 2 h (a) and 24 h (b). The reported values are the averages of two independent experiments, and are expressed as the relative fluorescence value to the control (untreated cells) which was assigned a value of 1. Differences were established using a One-way ANOVA followed by Dunnett *post hoc* test to compare every mean with the control, and considered significant at $P \leq 0.05$. *$P \leq 0.05$, **$P \leq 0.01$.
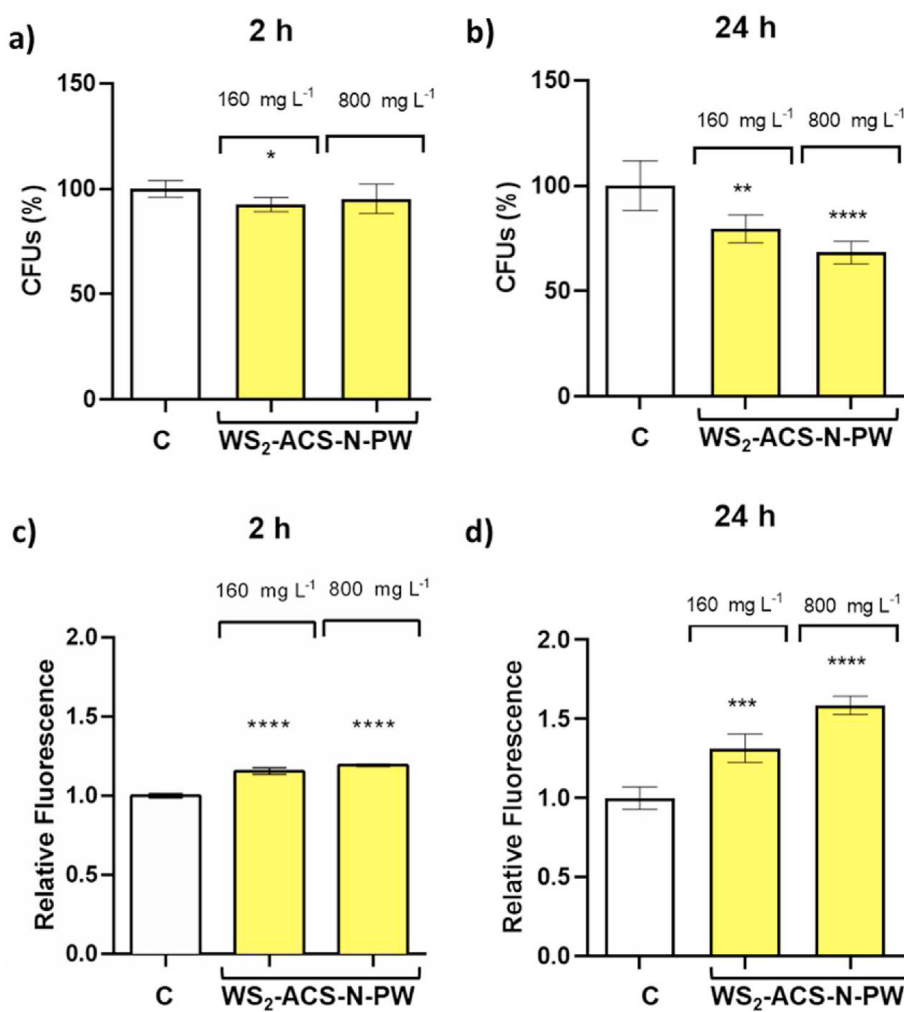

Fig. 8. CFUs and ROS determination of *S. cerevisiae* cells exposed to 160 and 800 mg L^{-1} of WS$_2$-ACS-N-PW, during 2 and 24 h. The reported values are the averages of two independent experiments. Differences were established using a One-way ANOVA followed by Dunnett *post hoc* test to compare every mean with the control, and considered significant at $P \leq 0.05$. *$P \leq 0.05$, **$P \leq 0.01$, ***$P \leq 0.001$, ****$P \leq 0.0001$.

dry form, which we named WS2-ACS-N-PW ("PW" standing for powder), reduced the viability of yeast too. Fig. 8 displays *S. cerevisiae* CFUs determination (Fig. 8a and b) and ROS assays (Fig. 8c and d), showing that the same concentrations of dry 2D WS_2 nanopowders aqueous suspensions and exposure conditions are able to produce a similar negative impact on *S. cerevisiae* cells viability. The different components identified in the analyzed commercial aqueous suspensions (1T'-WS_2, 2H-WS_2, WO_3, and sulphonyl groups), might have a role on their negative impact in yeast, which might be due to a mixture toxicity effect or through the action of one of the components identified. In particular, the antifungal properties of SO_2 are well known (KING et al., 1981).

4. Conclusions

The results obtained in the present work reveal the physico-chemical properties and the potential toxicity of commercial 2D WS_2 aqueous suspensions when interacting with distinct eukaryotic organisms, showing differences in function of the biological system exposed. Analysing the stoichiometry and structure of the nanomaterials it has been revealed that the particles are primarily monolayers, and they are composed by a combination of 1T'-WS_2, 2H-WS_2, WO_3 and SO_2 species. Toxicity analyses on human cells showed that both aqueous 2D WS_2 suspensions have not the ability to impact on their viability, and a small capacity to induce oxidative stress. The viability of *S. cerevisiae* was reduced in the presence of the nanomaterials after long exposure times, although their ability to trigger ROS production in this organism was very low. Additionally, the obtained results indicated that the same concentrations of aqueous suspensions prepared with dry 2D WS_2 nanopowders, employing comparable exposure conditions, are able to produce a similar toxicity impact on *S. cerevisiae* cells.

Author contributions

Brixhilda Domi: Investigation, Formal analysis, Writing — original draft - Review & Editing. Kapil Bhorkar: Investigation, Formal analysis, Writing — review & editing. Carlos Rumbo: Investigation, Formal analysis, Review & Editing. Labrini Sygellou: Investigation, Formal analysis, Review. Sonia Martel Martin: Resources, Review & Editing. Roberto Quesada: Supervision, Review & Editing. Spyros N. Yannopoulos: Resources, Methodology, Supervision, Writing — review & editing. Juan Antonio Tamayo-Ramos: Resources, Conceptualization, Methodology, Validation, Formal analysis, Investigation, Writing - Final Draft, Review & Editing, Supervision.

Funding sources

Declaration of competing interest

The authors declare that they have no known competing financial interests or personal relationships that could have appeared to influence the work reported in this paper.

Acknowledgements

References

Appel, J.H., Li, D.O., Podlevsky, J.D., Debnath, A., Green, A.A., Wang, Q.H., Chae, J., 2016. Low cytotoxicity and genotoxicity of two-dimensional MoS2 and WS2. ACS Biomater. Sci. Eng. 2, 361—367. https://doi.org/10.1021/acsbiomaterials.5b00467.

Berkdemir, A., Gutiérrez, H.R., Botello-Méndez, A.R., Perea-López, N., Elías, A.L., Chia, C.I., Wang, B., Crespi, V.H., López-Urías, F., Charlier, J.C., Terrones, H., Terrones, M., 2013. Identification of individual and few layers of WS2 using Raman Spectroscopy. Sci. Rep. 3, 1—8. https://doi.org/10.1038/srep01755.

Braconi, D., Bernardini, G., Santucci, A., 2016. Saccharomyces cerevisiae as a model in ecotoxicological studies: a post-genomics perspective. J. Proteomics 137, 19—34. https://doi.org/10.1016/j.jprot.2015.09.001.

Chng, E.L.K., Pumera, M., 2015. Toxicity of graphene related materials and transition metal dichalcogenides. RSC Adv. https://doi.org/10.1039/c4ra12624f.

Choi, W., Choudhary, N., Han, G.H., Park, J., Akinwande, D., Lee, Y.H., 2017. Recent development of two-dimensional transition metal dichalcogenides and their applications. Mater. Today. https://doi.org/10.1016/j.mattod.2016.10.002.

Corazzari, I., Deorsola, F.A., Gulino, G., Aldieri, E., Bensaid, S., Turci, F., Fino, D., 2014. Hazard assessment of W and Mo sulphide nanomaterials for automotive use. J. Nanoparticle Res. https://doi.org/10.1007/s11051-014-2401-7.

Domi, B., Bhorkar, K., Rumbo, C., Sygellou, L., Yannopoulos, S.N., Quesada, R., Tamayo-Ramos, J.A., 2020a. Fate assessment of commercial 2D MoS2 aqueous dispersions at physicochemical and toxicological level. Nanotechnology 31, 445101. https://doi.org/10.1088/1361-6528/aba6b3.

Domi, B., Bhorkar, K., Rumbo, C., Sygellou, L., Yannopoulos, S.N., Quesada, R., Tamayo-Ramos, J.A., 2020b. Fate assessment of commercial 2D MoS2 aqueous dispersions at physicochemical and toxicological level. Nanotechnology 31, 445101. https://doi.org/10.1088/1361-6528/aba6b3.

Domi, B., Rumbo, C., García-Tojal, J., Elena Sima, L., Negroiu, G., Tamayo-Ramos, J.A., 2019. Interaction analysis of commercial graphene oxide nanoparticles with unicellular systems and biomolecules. Int. J. Mol. Sci. 21, 205. https://doi.org/10.3390/ijms21010205.

Eftekhari, A., 2017. Tungsten dichalcogenides (WS2, WSe2, and WTe2): materials chemistry and applications. J. Mater. Chem. A 18299—18325. https://doi.org/10.1039/C7TA04268J.

Holmström, K.M., Finkel, T., 2014. Cellular mechanisms and physiological consequences of redox-dependent signalling. Nat. Rev. Mol. Cell Biol. 15, 411—421. https://doi.org/10.1038/nrm3801.

Ivask, A., Kurvet, I., Kasemets, K., Blinova, I., Aruoja, V., Suppi, S., Vija, H., Kakinen, A., Titma, T., Heinlaan, M., Visnapuu, M., Koller, D., Kisand, V., Kahru, A., 2014. Size-dependent toxicity of silver nanoparticles to bacteria, yeast, algae, crustaceans and mammalian cells in vitro. PloS One 9. https://doi.org/10.1371/journal.pone.0102108.

Jeevanandam, J., Barhoum, A., Chan, Y.S., Dufresne, A., Danquah, M.K., 2018. Review on nanoparticles and nanostructured materials: history, sources, toxicity and regulations. Beilstein J. Nanotechnol. https://doi.org/10.3762/bjnano.9.98.

Katz, A., Redlich, M., Rapoport, L., Wagner, H.D., Tenne, R., 2006. Self-lubricating coatings containing fullerene-like WS2 nanoparticles for orthodontic wires and other possible medical applications. Tribol. Lett. 21, 135—139. https://doi.org/10.1007/s11249-006-9029-4.

King, A.D., Ponting, J.D., Sanshuck, D.W., Jackson, R., Mihara, K., 1981. Factors affecting death of yeast by sulfur dioxide. J. Food Protect. 44, 92—97. https://doi.org/10.4315/0362-028x-44.2.92.

Kwolek-Mirek, M., Zadrag-Tecza, R., 2014. Comparison of methods used for assessing the viability and vitality of yeast cells. FEMS Yeast Res. 14, 1068—1079. https://doi.org/10.1111/1567-1364.12202.

Lanone, S., Rogerieux, F., Geys, J., Dupont, A., Maillot-Marechal, E., Boczkowski, J., Lacroix, G., Hoet, P., 2009. Comparative toxicity of 24 manufactured nanoparticles in human alveolar epithelial and macrophage cell lines. Part. Fibre Toxicol. 6, 1—12. https://doi.org/10.1186/1743-8977-6-14.

Liu, X., Duan, G., Li, W., Zhou, Z., Zhou, R., 2017. Membrane destruction-mediated antibacterial activity of tungsten disulfide (WS2). RSC Adv. 7, 37873—37880. https://doi.org/10.1039/c7ra06442j.

Liu, Z., Li, N., Su, C., Zhao, H., Xu, L., Yin, Z., Li, J., Du, Y., 2018. Colloidal synthesis of 1T' phase dominated WS2 towards endurable electrocatalysis. Nano Energy 50, 176—181. https://doi.org/10.1016/j.nanoen.2018.05.019.

Lv, R., Robinson, J.A., Schaak, R.E., Sun, D., Sun, Y., Mallouk, T.E., Terrones, M., 2015. Transition metal dichalcogenides and beyond: synthesis, properties, and applications of single- and few-layer nanosheets. Acc. Chem. Res. 48, 56—64. https://doi.org/10.1021/ar5002846.

Marletta, G., Iacona, F., 1996. Chemical selectivity and energy transfer mechanisms in the radiation-induced modification of polyethersulphone. Nucl. Instrum. Methods Phys. Res. Sect. B Beam Interact. Mater. Atoms 116, 246—252. https://doi.org/10.1016/0168-583X(96)00041-9.

Mell, J.C., Burgess, S.M., 2002. Yeast as a Model Genetic Organism.

Michels, C.A., 2003. Saccharomyces cerevisiae as a genetic model organism. Genet. Tech. Biol. Res. 6, 1—22. https://doi.org/10.1002/0470846623.ch1.

Pardo, M., Shuster-Meiseles, T., Levin-Zaidman, S., Rudich, A., Rudich, Y., 2014. Low cytotoxicity of inorganic nanotubes and fullerene-like nanostructures in human bronchial epithelial cells: relation to inflammatory gene induction and antioxidant response. Environ. Sci. Technol. 48 https://doi.org/10.1021/es500065z.

Peng, Q., Huo, D., Li, H., Zhang, B., Li, Y., Liang, A., Wang, H., Yu, Q., Li, M., 2018. ROS-independent toxicity of Fe3O4 nanoparticles to yeast cells: involvement of

mitochondrial dysfunction. Chem. Biol. Interact. 287, 20–26. https://doi.org/10.1016/j.cbi.2018.03.012.

Perrone, G.G., Tan, S.X., Dawes, I.W., 2008. Reactive oxygen species and yeast apoptosis. Biochim. Biophys. Acta Mol. Cell Res. 1783, 1354–1368. https://doi.org/10.1016/j.bbamcr.2008.01.023.

Ratoi, M., Niste, V.B., Walker, J., Zekonyte, J., 2013. Mechanism of action of WS2 lubricant nanoadditives in high-pressure contacts. Tribol. Lett. 52, 81–91. https://doi.org/10.1007/s11249-013-0195-x.

Repetto, G., del Peso, A., Zurita, J.L., 2008. Neutral red uptake assay for the estimation of cell viability/cytotoxicity. Nat. Protoc. 3, 1125–1131. https://doi.org/10.1038/nprot.2008.75.

Sharma, P., Kumar, A., Bankuru, S., Chakraborty, J., Puravankara, S., 2020. Large-scale surfactant-free synthesis of WS2 nanosheets: an investigation into the detailed reaction chemistry of colloidal precipitation and their application as an anode material for lithium-ion and sodium-ion batteries. New J. Chem. 44, 1594–1608. https://doi.org/10.1039/c9nj04662c.

Sousa, C.A., Soares, H.M.V.M., Soares, E.V., 2018. Nickel oxide (NiO) nanoparticles induce loss of cell viability in yeast mediated by oxidative stress. Chem. Res. Toxicol. 31, 658–665. https://doi.org/10.1021/acs.chemrestox.8b00022.

Sousa, C.A., Soares, H.M.V.M., Soares, E.V., 2019. Metal(loid) oxide (Al2O3, Mn3O4, SiO2 and SnO2) nanoparticles cause cytotoxicity in yeast via intracellular generation of reactive oxygen species. Appl. Microbiol. Biotechnol. 103, 6257–6269. https://doi.org/10.1007/s00253-019-09903-y.

Štengl, V., Henych, J., Slušná, M., Ecorchard, P., 2014. Ultrasound exfoliation of inorganic analogues of graphene. Nanoscale Res. Lett. 9, 1–14. https://doi.org/10.1186/1556-276X-9-167.

Tan, S.J.R., Abdelwahab, I., Ding, Z., Zhao, X., Yang, T., Loke, G.Z.J., Lin, H., Verzhbitskiy, I., Poh, S.M., Xu, H., Nai, C.T., Zhou, W., Eda, G., Jia, B., Loh, K.P., 2017. Chemical stabilization of 1T′ phase transition metal dichalcogenides with giant optical kerr nonlinearity. J. Am. Chem. Soc. 139, 2504–2511. https://doi.org/10.1021/jacs.6b13238.

Teo, W.Z., Chng, E.L.K., Sofer, Z., Pumera, M., 2014. Cytotoxicity of exfoliated transition-metal dichalcogenides (MoS 2 , WS 2 , and WSe 2) is lower than that of graphene and its analogues. Chem. Eur J. 20, 9627–9632. https://doi.org/10.1002/chem.201402680.

Visalli, G., Bertuccio, M.P., Iannazzo, D., Piperno, A., Pistone, A., Di Pietro, A., 2015. Toxicological assessment of multi-walled carbon nanotubes on A549 human lung epithelial cells. Toxicol. Vitro 29, 352–362. https://doi.org/10.1016/J.TIV.2014.12.004.

Yuan, P., Zhou, Q., Hu, X., 2020. WS2 nanosheets at noncytotoxic concentrations enhance the cytotoxicity of organic pollutants by disturbing the plasma membrane and efflux pumps. Environ. Sci. Technol. 54, 1698–1709. https://doi.org/10.1021/acs.est.9b05537.

Yuan, P., Zhou, Q., Hu, X., 2018. The phases of WS2 nanosheets influence uptake, oxidative stress, lipid peroxidation, membrane damage, and metabolism in algae. Environ. Sci. Technol. 52, 13543–13552. https://doi.org/10.1021/acs.est.8b04444.

Zirak, M., Zhao, M., Moradlou, O., Samadi, M., Sarikhani, N., Wang, Q., Zhang, H.L., Moshfegh, A.Z., 2015. Controlled engineering of WS2 nanosheets-CdS nanoparticle heterojunction with enhanced photoelectrochemical activity. Sol. Energy Mater. Sol. Cells 141, 260–269. https://doi.org/10.1016/j.solmat.2015.05.051.